Available online at www.sciencedirect.com
SCIENCE DIRECT®
International Journal of Heat and Mass Transfer 48 (2005) 2064–2078
International Journal of HEAT and MASS TRANSFER
www.elsevier.com/locate/ijhmt

Momentum functions and momentum lines for fluid flow visualization and analysis

V.A.F. Costa *

Departamento de Engenharia Mecânica, Universidade de Aveiro, Campus Universitário de Santiago, 3810-193 Aveiro, Portugal

Received 13 April 2004
Available online 26 February 2005

Abstract

Heat lines and mass lines are well established as powerful tools for visualization and analysis of two-dimensional convective heat and/or mass transfer. These tools were proposed in the eighties, and their use and range of use in the field of convective heat and/or mass transfer have grown since they were proposed. In this work, a new field based on the momentum functions and momentum lines is proposed for steady flow visualization and analysis. As momentum is a vector entity, two momentum functions need to be defined and evaluated, one for each momentum component. The contour plots of the momentum functions, the momentum lines, are the useful tools for flow visualization and analysis. Additionally, momentum arrows can also be used for visualization purposes. Such tools provide a clear physical insight about the momentum transfer in flows, and important information concerning the forces between the fluid and the solid walls interacting with it. Some illustrative examples are presented in order to show the usefulness of the momentum lines for flow visualization and analysis.

1. Introduction

The heatfunction and heat lines were proposed by Kimura and Bejan [1] as the adequate tools for convective heat transfer visualization. Before that, the heat flux lines were routinely used for analyzing pure conduction heat transfer in isotropic media [2], the heat flux lines being perpendicular to the isotherms. The heatfunction and heat lines are the convective heat transfer counterpart of the streamfunction and stream lines, used for long time for visualization and analysis of flow problems, the heat lines defining well bordered corridors (energy tubes) where energy flows. The concept evolved to problems involving convective mass transfer, through the introduction of the massfunction and mass lines by Trevisan and Bejan [3]. As the mass and energy conservation equations are the same in open fluid domains and in porous domains, the heat lines and mass lines can be equally applied when dealing with convective heat and/or mass transfer problems in porous domains.

Several improvements were made to enlarge the applicability range of the heat lines and mass lines. Such improvements include the use of the heat lines in cylindrical systems [4], and unsteady problems [5,6]. Also the similarity solutions for the heatfunction were obtained for laminar boundary layer problems under different heating or cooling conditions, including forced convection near a flat plate [7], forced convection near a flat plate in a fluid saturated porous medium [8], and natural convection near a vertical flat plate [9]. The heat

* Tel.: +351 234 370 829; fax: +351 234 370 953.
E-mail address: v_costa@mec.ua.pt

0017-9310/$ - see front matter © 2005 Elsevier Ltd. All rights reserved.
doi:10.1016/j.ijheatmasstransfer.2004.12.014

Nomenclature

C_f	skin-friction coefficient
D	width
D_h	hydraulic diameter
f	friction factor
f	similarity function
F	force
g	gravitational acceleration
g	auxiliary function
H	height
L	length
M	momentum function
n	auxiliary coefficient
p	pressure
Re	Reynolds number
s	segment
U	inlet or reference velocity
u, v	Cartesian velocity components
x, y	Cartesian co-ordinates
X	momentum transfer parameter

Greek symbols

δ	boundary layer thickness
δ	Kronecker's delta
η	similarity variable
θ	angle (surface orientation)
μ	dynamic viscosity
ρ	density
σ	stress component
τ	stress
ψ	streamfunction

Subscripts

D	referring width D
i, j, k	Cartesian indices
L	referring length L
n	normal
ob	obstacle
r	reference value
t	tangential
x, y	referring Cartesian co-ordinates
0	reference value
*	dimensionless
∞	free stream value

Superscript

x, y	referring Cartesian directions

line concept was developed for turbulent flows, using the turbulent flux components [10] or an effective diffusion coefficient that includes the eddy diffusivity for heat transfer when dealing with turbulent boundary layer flows [11]. A unified formulation was proposed for the stream line, heat line and mass line methods [12], with special emphasis on the diffusion coefficients for these functions if adjacent media of different properties are present. In this way, a unified treatment is available to be incorporated into software packages for heat and/or mass transfer and fluid flow. The unified treatment has been extended to deal with convection in anisotropic fluid saturated porous media [13]. These visualization tools can be applied when the mass and energy governing differential equations are divergence-free, and thus only recently they were applied to reacting flows [14,15]. In this case, in order to have divergence-free equations, the selected conserved scalars are the total enthalpy (enthalpy of formation plus sensible enthalpy) and the elemental mass fractions. In the first work [14], special (and involved) forms of the conservation equations and of their transport coefficients need to be incorporated. In a more recent work, a unified treatment is proposed to deal with reacting flows, which is simpler and physically consistent [15]. A recent review on the heat line and mass line methods can be found in [16].

The steady momentum equations, without source term, can also be treated as divergence-free, noting that the pressure gradient term is a surface term and not a volumetric term. It should be noted, however, that the pressure gradient term is usually referred to as a momentum source term, even if it is not a true source term. Once the momentum equations are represented in this way, one can obtain the momentum functions, whose contour plots, i.e. the momentum lines, are very useful tools for flow visualization and analysis. Once known the momentum functions, they can be used to obtain pictures, in the form of momentum arrows, which can be equally important for visualization and analysis. Usually, the flow problems are visualized and analyzed through the stream lines (defining mass tubes), which are very useful to have a good picture of flow kinetics, but they do not provide any indication how the forces within the fluid interact, and how the fluid interacts with the walls containing it. The momentum lines provide a very clear physical insight about these interactions, in the form of forces, which are of great value for flow visualization and analysis. When compared with the stream lines, heat lines and mass lines, some additional care needs to be taken due to the vector nature of the forces, and regarding the conventions used to analyze the stress components and their associated forces.

2. Physical modeling

2.1. Equations governing 2D steady incompressible flows

The 2D steady incompressible flow problems in open fluid domains are governed by the mass conservation equation, that can be written using the indicial notation as

$$\frac{\partial}{\partial x_i}(\rho u_i) = 0 \tag{1}$$

and by the momentum equations [17]

$$\frac{\partial}{\partial x_i}(\rho u_i u_j) = -\frac{\partial (p - p_0)}{\partial x_j} + \frac{\partial \tau_{ij}}{\partial x_i} \tag{2}$$

where the tensor stress components, for a Newtonian fluid, are obtained as

$$\tau_{ij} = \mu\left(\frac{\partial u_i}{\partial x_j} + \frac{\partial u_j}{\partial x_i}\right) - \frac{2}{3}\mu\frac{\partial u_k}{\partial x_k}\delta_{ij} \tag{3}$$

The reference value for the pressure, p_0, is arbitrarily chosen, as the pressure level is irrelevant when dealing with incompressible flow problems. In this work, p_0 is taken as the minimum pressure value in the domain, the acting pressure is always positive, thus giving rise to compressive stresses only. Pressure present in Eq. (2) is the driving pressure, which effectively drives the flow, obtained as the total real pressure plus the hydrostatic pressure, that is, $p = p_{\text{real}} + \rho g y$, where the gravitational acceleration g points downward in the y direction [17]. If the real force over the domain boundaries is to be evaluated, both the hydrostatic pressure and the reference pressure should be taken into account. For non-polar fluids $\tau_{ij} = \tau_{ji}$. If the fluid is incompressible, the term $\partial u_k/\partial x_k$ vanishes in Eq. (3), invoking the mass conservation equation, Eq. (1), what corresponds to the situations considered in this work.

For the 2D situations, the mass conservation equation can be rewritten as

$$\frac{\partial}{\partial x}(\rho u) + \frac{\partial}{\partial y}(\rho v) = 0 \tag{4}$$

and the momentum equations can be rewritten as

$$\frac{\partial}{\partial x}[\rho u u + (p - p_0) - \tau_{xx}] + \frac{\partial}{\partial y}(\rho u v - \tau_{xy}) = 0 \tag{5}$$

$$\frac{\partial}{\partial x}(\rho u v - \tau_{xy}) + \frac{\partial}{\partial y}[\rho v v + (p - p_0) - \tau_{yy}] = 0 \tag{6}$$

The stress tensor components are obtained from Eq. (3) as

$$\tau_{xx} = 2\mu\frac{\partial u}{\partial x}; \quad \tau_{yy} = 2\mu\frac{\partial v}{\partial y};$$
$$\tau_{xy} = \tau_{yx} = \mu\left(\frac{\partial u}{\partial y} + \frac{\partial v}{\partial x}\right) \tag{7}$$

2.2. Momentum functions and momentum lines

From Eq. (5) one can define the momentum function M^x, in the co-ordinate direction x, through its first-order derivatives as

$$\frac{\partial M^x}{\partial y} = \rho u u + (p - p_0) - \tau_{xx} \tag{8a}$$

$$-\frac{\partial M^x}{\partial x} = \rho u v - \tau_{xy} \tag{8b}$$

Equating the second-order mixed derivatives of M^x, assuming that M^x is a continuous function to its second-order derivatives, Eq. (5) is satisfied identically.

Similarly, from Eq. (6) one can define the momentum function M^y, in the co-ordinate direction y, through its first-order derivatives as

$$\frac{\partial M^y}{\partial y} = \rho u v - \tau_{xy} \tag{9a}$$

$$-\frac{\partial M^y}{\partial x} = \rho v v + (p - p_0) - \tau_{yy} \tag{9b}$$

Again, equating the second-order mixed derivatives of M^y and assuming that M^y is a continuous function to its second-order derivatives, Eq. (6) is satisfied identically. Having defined the momentum functions corresponding to the two Cartesian co-ordinate directions, some explanation is given about its physical meaning and interpretation.

The total differential of the momentum function M^x can be obtained, invoking Eqs. (8a) and (8b), as

$$\begin{aligned} \mathrm{d}M^x &= \frac{\partial M^x}{\partial x}\mathrm{d}x + \frac{\partial M^x}{\partial y}\mathrm{d}y \\ &= -(\rho u v - \tau_{xy})\,\mathrm{d}x + [\rho u u + (p - p_0) - \tau_{xx}]\,\mathrm{d}y \end{aligned} \tag{10}$$

and the total differential of the momentum function M^y can be obtained, invoking Eqs. (9a) and (9b), as

$$\begin{aligned} \mathrm{d}M^y &= \frac{\partial M^y}{\partial x}\mathrm{d}x + \frac{\partial M^y}{\partial y}\mathrm{d}y \\ &= -[\rho v v + (p - p_0) - \tau_{yy}]\,\mathrm{d}x + (\rho u v - \tau_{xy})\,\mathrm{d}y \end{aligned} \tag{11}$$

These total differentials can be physically interpreted considering Fig. 1, where the stress components existing at a given point are presented for a differential control element with a unit depth [18]. The condition of equilibrium in the x direction gives that

$$\begin{aligned} \sigma_x\,\mathrm{d}s &= -(\rho u v - \tau_{xy})\,\mathrm{d}x + [\rho u u + (p - p_0) - \tau_{xx}]\,\mathrm{d}y \\ &= \mathrm{d}M^x \end{aligned} \tag{12}$$

and the condition of equilibrium in the y direction gives that

$$\begin{aligned} \sigma_y\,\mathrm{d}s &= -[\rho v v + (p - p_0) - \tau_{yy}]\,\mathrm{d}x + (\rho u v - \tau_{xy})\,\mathrm{d}y \\ &= \mathrm{d}M^y \end{aligned} \tag{13}$$

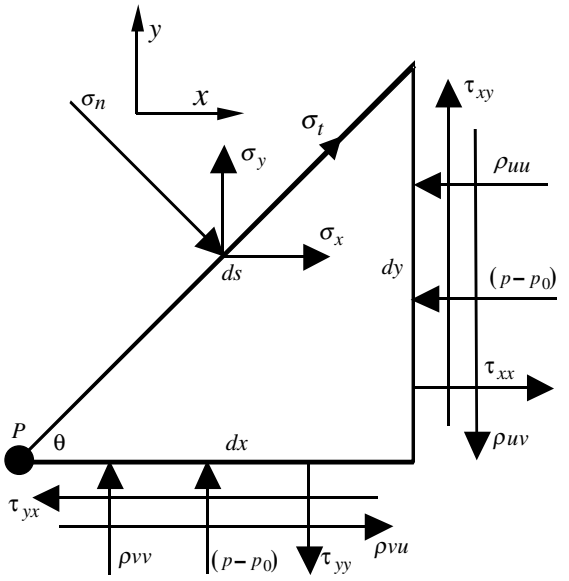

Fig. 1. Evaluation of the stress components σ_x and σ_y acting over a differential surface of unit depth.

There are two important observations from these results. The difference in the momentum function M^x, corresponding to two points 1 and 2 in the domain, gives the additional force in the x direction, per unit depth, encountered when traveling from point 1 to point 2. It also implies that a line of constant M^x, a contour plot of M^x, where $dM^x = 0$, is a line along which there is no stress (or force) in the x direction. The region between two lines of constant values of M^x can then be seen as a beam, whose surface is not subjected to applied forces in the x direction. There are the lines of constant M^x, the x momentum lines, which provide a useful tool for flow visualization and analysis of the existing interactions in the flow, in the form of forces. Similar conclusions can be extracted for the momentum function M^y, whose contour plots are the y momentum lines. In this case, the region between two lines of constant values of M^y can be seen as a beam, whose surface is not subjected to applied forces in the y direction.

Additionally, the momentum functions can be used to obtain momentum arrows, and thus to another way for flow visualization and analysis. For the considered cases, however, pictures given by the momentum lines are much better than the ones given by the momentum arrows.

2.3. Differential equations for the momentum functions

The differential equation for the x momentum function M^x can be obtained from Eqs. (8a) and (8b), evaluating and adding the second-order derivatives of M^x, resulting in the Poisson equation

$$\frac{\partial^2 M^x}{\partial x^2}+\frac{\partial^2 M^x}{\partial y^2}=-\frac{\partial}{\partial x}(\rho uv)+\frac{\partial}{\partial y}(\rho uu)+\frac{\partial (p-p_0)}{\partial y}-\left\{2\frac{\partial}{\partial y}\left(\mu\frac{\partial u}{\partial x}\right)-\frac{\partial}{\partial x}\left[\mu\left(\frac{\partial u}{\partial y}+\frac{\partial v}{\partial x}\right)\right]\right\} \tag{14}$$

If the dynamic viscosity μ can be taken as constant, Eq. (14) becomes

$$\frac{\partial^2 M^x}{\partial x^2}+\frac{\partial^2 M^x}{\partial y^2}=-\frac{\partial}{\partial x}(\rho uv)+\frac{\partial}{\partial y}(\rho uu)+\frac{\partial (p-p_0)}{\partial y}-\mu\frac{\partial}{\partial x}\left(\frac{\partial u}{\partial y}-\frac{\partial v}{\partial x}\right) \tag{15}$$

The differential equation for the momentum function M^y can be obtained similarly from Eqs. (9a) and (9b) as

$$\frac{\partial^2 M^y}{\partial x^2}+\frac{\partial^2 M^y}{\partial y^2}=-\frac{\partial}{\partial x}(\rho vv)+\frac{\partial}{\partial y}(\rho uv)-\frac{\partial (p-p_0)}{\partial x}-\left\{\frac{\partial}{\partial y}\left[\mu\left(\frac{\partial u}{\partial y}+\frac{\partial v}{\partial x}\right)\right]-2\frac{\partial}{\partial x}\left(\mu\frac{\partial v}{\partial y}\right)\right\} \tag{16}$$

or, taking the dynamic viscosity as constant,

$$\frac{\partial^2 M^y}{\partial x^2}+\frac{\partial^2 M^y}{\partial y^2}=-\frac{\partial}{\partial x}(\rho vv)+\frac{\partial}{\partial y}(\rho uv)-\frac{\partial (p-p_0)}{\partial x}-\mu\frac{\partial}{\partial y}\left(\frac{\partial u}{\partial y}-\frac{\partial v}{\partial x}\right) \tag{17}$$

These are the differential equations that are solved, once the flow field is solved, to obtain the momentum function fields. It can be mentioned that the last term within brackets in Eqs. (15) and (17) is the symmetric of one-half of the rotational of the velocity field, that is, $(\partial u/\partial y - \partial v/\partial x) = -2\varpi_z$, where $\varpi_z = (1/2)\nabla \times \mathbf{V}$.

It should be noted that, for a fluid of constant density and viscosity, the momentum equations could be written in the form of Eqs. (5) and (6) as [11,18]

$$\frac{\partial}{\partial x}\left[\rho uu+(p-p_0)-\mu\frac{\partial u}{\partial x}\right]+\frac{\partial}{\partial y}\left(\rho uv-\mu\frac{\partial u}{\partial y}\right)=0 \tag{18a}$$

$$\frac{\partial}{\partial x}\left(\rho uv-\mu\frac{\partial v}{\partial x}\right)+\frac{\partial}{\partial y}\left[\rho vv+(p-p_0)-\mu\frac{\partial v}{\partial y}\right]=0 \tag{18b}$$

and it is tempting to define the momentum functions, through their first-order derivatives, using the terms within brackets in Eqs. (18a) and (18b). However, the corresponding terms in the original equations, Eqs. (5) and (6), are different from the terms in the momentum equations as given by Eqs. (18a) and (18b). This difference is due to simplifications made in the momentum equations, using the mass conservation equation, that are possible due to the derivatives present in the viscous

terms of Eqs. (5) and (6). But the true, and total stress terms are those in the original momentum equations, Eqs. (5) and (6), and the momentum functions must be defined through their first-order derivatives using the original Eqs. (5) and (6), and not from the simplified Eqs. (18a) and (18b).

2.4. Boundary conditions for the momentum functions

Since momentum functions M^x and M^y are defined through its first-order derivatives (Eqs. (8) and (9)), only differences on their values are important, and not their levels. As the momentum functions are evaluated, once the flow field is solved, using available analytical or numerical techniques, the flow solution at the boundaries is used to set the boundary values of the momentum functions. This is illustrated for the M^x momentum function, in a rectangular domain, and a similar procedure can be used for other domains and also for the M^y momentum function.

At an arbitrary reference point at the boundary, (x_r, y_r), the momentum function is set to be $M^x(x_r, y_r) = 0$ or it is known by any way. If the reference point (x_r, y_r) is over a horizontal boundary, the M^x value over any point of such boundary is set, from Eq. (8b), as

$$M^x(x, y_r) = M^x(x_r, y_r) - \int_{x_r}^{x} (\rho uv - \tau_{xy})\,\mathrm{d}x \tag{19}$$

If $u = 0$ or $v = 0$ at such a boundary, then Eq. (19) becomes

$$M^x(x, y_r) = M^x(x_r, y_r) + \int_{x_r}^{x} \mu(\partial u/\partial y + \partial v/\partial x)\,\mathrm{d}x \tag{20}$$

If the reference point (x_r, y_r) is over a vertical boundary, the M^x value over any point of such boundary is set, from Eq. (8a), as

$$M^x(x_r, y) = M^x(x_r, y_r) + \int_{y_r}^{y} [\rho uu + (p - p_0) - \tau_{xx}]\,\mathrm{d}y \tag{21}$$

If $u = 0$ at this vertical boundary, Eq. (21) becomes

$$M^x(x_r, y) = M^x(x_r, y_r) + \int_{y_r}^{y} [(p - p_0) - 2\mu(\partial u/\partial x)]\,\mathrm{d}y \tag{22}$$

At this point some attention should be given to the physical significance of the boundary conditions as specified in Eqs. (20) and (22), corresponding to boundary conditions at a solid impermeable boundary ($u = v = 0$). The physical insight is more relevant at these boundaries, as they are routinely studied in fluid dynamics. Similar considerations can be made also for the boundary conditions pertaining to the momentum function M^y. Along the horizontal boundary $\partial v/\partial x = 0$, and Eq. (20) gives $M^x(x, y_r) = M^x(x_r, y_r) + \int_{x_r}^{x} \mu(\partial u/\partial y)\,\mathrm{d}x$. It is well known that, at such a boundary, the shear stress is $\mu(\partial u/\partial y)$, and the variation of the momentum function M^x from x_r to x is the applied boundary shear force, by unit depth. At this horizontal boundary, the force induced by pressure in the x direction is absent. Along the vertical boundary, the normal stress in the x direction is $-2\mu(\partial u/\partial x)$, and the x-direction force induced by pressure exists, the total normal stress being $[(p - p_0) - 2\mu(\partial u/\partial x)]$. In this way, the variation of the momentum function M^x from y_r to y is the applied normal boundary force, by unit depth.

If the boundary is inclined relative to the Cartesian co-ordinate system, like the situation presented at the differential level in Fig. 1, the expression for the normal (compressive) stress, σ_n, can be obtained as

$$\sigma_n = \frac{1}{2}(\rho uu - \tau_{xx})(1 - \cos 2\theta) + \frac{1}{2}(\rho vv - \tau_{yy})(1 + \cos 2\theta) + (p - p_0) - (\rho uv - \tau_{xy}) \sin 2\theta \tag{23}$$

and the expression for the tangential stress, σ_t, in the direction away from the pivotal point P in Fig. 1, is

$$\sigma_t = -(\rho uv - \tau_{xy}) \cos 2\theta + \frac{1}{2}(\rho uu - \tau_{xx} - \rho vv + \tau_{yy}) \sin 2\theta \tag{24}$$

As expected, pressure acts always as a compressive stress, and does not give any contribution to the tangential stress. The state of stress for a surface with a given orientation can be obtained applying Eqs. (23) and (24), and the results for the different faces of a differential element are presented in Fig. 2. Special care is needed when analyzing the stresses, because their signs are dependent on the orientation of the considered surface, as shown in Fig. 2.

Momentum functions were presented and discussed in the context of viscous flows. However, they can be

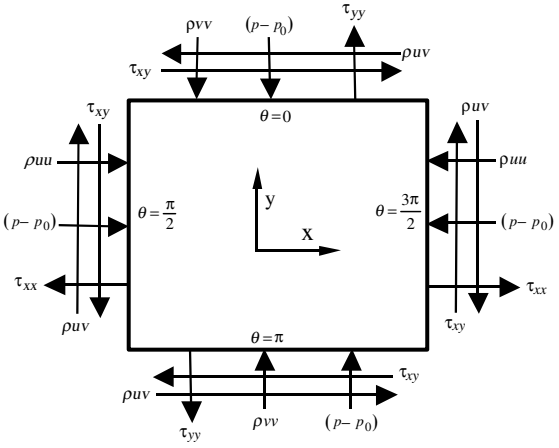

Fig. 2. Stress components at the faces with different orientation angles.

equally applied for inviscid flows. In that case, the foregoing results apply with $\mu = 0$ (zero shear stress), and the momentum functions give a picture of the interplaying inertial and pressure forces.

3. Illustrations

In order to illustrate the use of the momentum functions and momentum lines for flow visualization and analysis, four simple laminar flow problems are considered: (i) Couette flow between parallel plates, without pressure gradient, (ii) fully developed laminar flow between parallel plates, (iii) forced boundary layer flow over a flat plate (similarity solution for the momentum function), and (iv) forced flow in a channel with an obstacle.

3.1. Couette flow between parallel plates, without pressure gradient

The domain under analysis is presented in Fig. 3, and consists of a horizontal channel of width D and length $L = D$, delimited by two parallel plates. The upper plate moves with uniform velocity U and the lower plate is at rest.

The flow is assumed to be laminar and fully developed, and all the fluid particles move in the direction parallel to the plates. From the vertical momentum equation it is obtained that $\partial p/\partial y = 0$. As the velocity component u is constant with x, the horizontal momentum equation reads $-\mathrm{d}p/\mathrm{d}x + \mu(\mathrm{d}^2u/\mathrm{d}y^2) = 0$. In this case, it is assumed that the flow moves due to shear only, and that pressure gradient is absent. The treatment of this problem including pressure gradient in the x direction can be found, for example, in Ref. [18]. Making the y co-ordinate dimensionless as $y_* = y/D$ and the velocity dimensionless as $u_* = u/U$, the dimensionless velocity profile is

$$u_* = y_* \tag{25}$$

Noting that the pressure is constant, and $(p - p_0) = 0$, from Eqs. (8a) and (8b) the momentum function M^x is defined through $(\partial M^x/\partial y) = \rho uu$ and $-(\partial M^x/\partial x) = -\mu(\mathrm{d}u/\mathrm{d}y)$. Making the momentum function dimensionless as $M^x_* = M^x/(\rho U^2 D)$, and using Eq. (25), the dimensionless momentum function M^x_* is defined through

$$\frac{\partial M^x_*}{\partial y_*} = y_*^2 \tag{26a}$$

$$\frac{\partial M^x_*}{\partial x_*} = (1/Re_D) \tag{26b}$$

where $Re_D = \rho UD/\mu$.

From Eqs. (26a) and (26b), the analytical solution for the dimensionless momentum function M^x_* is obtained as

$$M^x_*(x_*, y_*) = \frac{1}{3}y_*^3 + \frac{1}{Re_D}x_* \tag{27}$$

once set that $M^x_*(0,0) = 0$.

Similarly, the momentum function M^y, defined from Eqs. (9a) and (9b) is obtained through $(\partial M^y/\partial y) = -\mu(\mathrm{d}u/\mathrm{d}y)$ and $-(\partial M^y/\partial x) = 0$, and M^y is function of y only. The dimensionless version of the differential equation for M^y_* is thus

$$\frac{\mathrm{d}M^y_*}{\mathrm{d}y_*} = -\frac{1}{Re_D} \tag{28}$$

whose analytical solution gives

$$M^y_*(x_*, y_*) = -\frac{1}{Re_D}y_* \tag{29}$$

once verified that $M^y_*(0,0) = 0$.

It should be noted here that if the M^y momentum function was defined from the simplified y momentum equation, Eq. (18b), it would give $\partial M^y/\partial y = 0$. In fact, if the shear stress $\tau_{yx} = \mu\,(\partial u/\partial y)$ exists in the x direction, by the principle of reciprocity of the shear stresses this same shear stress also exists in the y direction. However, as the velocity profile does not change with x, the term $\partial/\partial x[\mu(\partial u/\partial y)]$ vanishes in the y momentum equation. But, in reality, the shear stress in the y direction exists, and it is taken correctly into account in the momentum function definition if the original momentum equations, Eqs. (5) and (6), are taken.

Results obtained for the dimensionless momentum functions M^x_* and M^y_* are presented in Fig. 4a–c. It is observed from Fig. 4a and c that the momentum function M^x_* increases uniformly with x_*, as expected from Eq. (26b). It is observed that this increase is more intense for lower values of the Reynolds number (higher viscosity fluids). It is also observed that the slope of the momentum lines is constant at the upper and lower plates, as indicated from Eq. (26a) for constant values of y_*. In particular, this slope is null for $y_* = 0$, similarly to what happens with the heatfunction near impermeable isothermal walls [12].

At the upper boundary of the fluid, the shear stress points in the x_* direction, what corresponds to a positive σ_x in Fig. 1 for $\theta = 0$, and the momentum function M^x_*

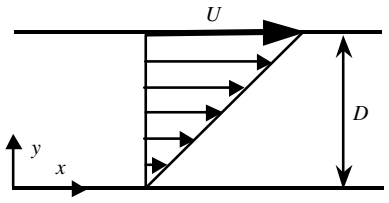

Fig. 3. Physical model and geometry for the Couette flow problem.

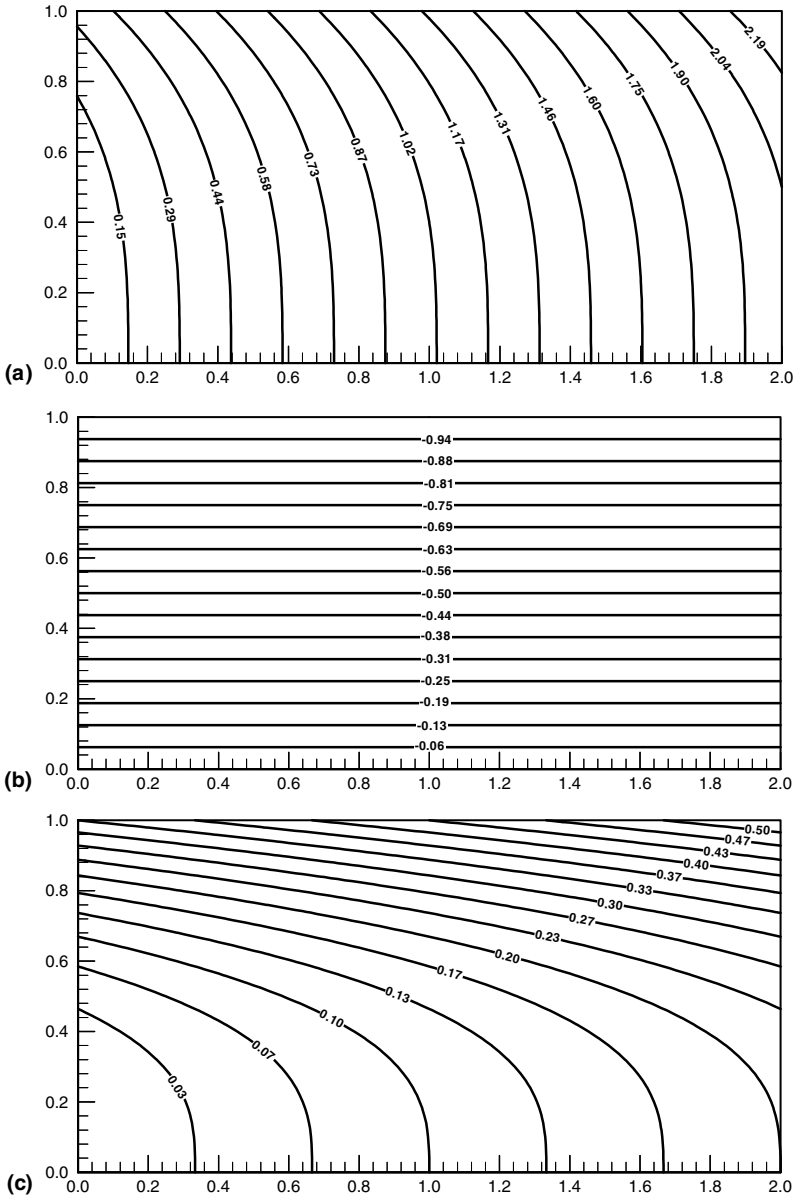

Fig. 4. Dimensionless momentum lines for the Couette flow problem: (a) momentum lines M_*^x for $Re_D = 1$; (b) momentum lines M_*^y for $Re_D = 1$ and (c) momentum lines M_*^x for $Re_D = 10$.

increases with x_* at the upper plate, for which $y_* = 1$. At the lower boundary of the fluid, the shear stress points in the $-x_*$ direction, what corresponds to a negative σ_x in Fig. 1 for $\theta = \pi$, and to a positive shear stress there, and the momentum function M_*^x also increases with x_* at the lower plate, for which $y_* = 0$. Lines of constant momentum function M_*^x are lines where the stress (or force) in the x_* direction is zero, and the region between two of such momentum lines can be seen as a beam in which surface (exception made to the boundary domain surfaces) there are no applied forces in the x_* direction, as illustrated in Fig. 5. Along such a beam, the force in the x_* direction is transmitted through action–reaction pairs of forces, in accordance with the Newton's third law. The overall dimensionless force acting in the x_* direction, over the upper and lower plates, can be easily obtained as the respective overall difference in the dimensionless momentum function M_*^x.

It is also observed that the inertial terms become more important as the Reynolds number increases, by

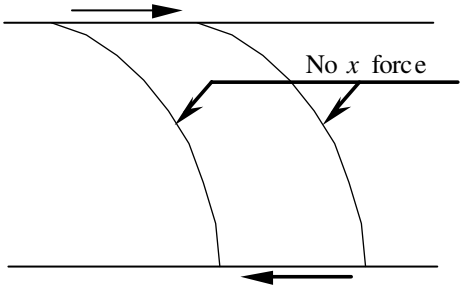

Fig. 5. Illustration of the region between two momentum lines of M_*^x as a beam without surface stresses or forces.

comparing Fig. 4a and c. When viscous effects are higher, as in Fig. 4a, the momentum in the x_* direction is transferred from the moving upper plate to the lower plate by fluid beams, which are nearly vertical. However, for higher Reynolds number, the momentum in the x_* direction is transferred from the moving upper plate to the lower plate by fluid beams with high inclination. In this case, the forces are transmitted through long lengths, along the so-called fluid beams. The inertial inlet of momentum in the x_* direction can be obtained by analyzing the increase of the dimensionless momentum function M_*^x along a vertical surface of Fig. 4a or c.

Regarding momentum function M_*^y, presented in Fig. 4b, it is observed that it decreases with y_*, as expected from Eq. (29). The shear stress in this flow, the only stress component in the y_* direction is $\tau_{xy,*} = 1/Re_D$, and positive in the whole domain, but it points downward when analyzing the left side of the vertical face of a differential element, and it points upward when analyzing the right side of the vertical face of the same differential element. As such stresses point in opposite senses of a differential element, they do not give rise to any resulting force in the y_* direction. Another way to interpret these results is to see from Fig. 4b that, at the upper or lower boundaries, there is no change of the momentum function, and thus there is no resulting net force in the y direction acting over such boundaries. From Fig. 2 it can be seen that the left face of a differential element corresponds to $\theta = \pi/2$, and, at such a face, σ_y points upward. From Fig. 2, for $\theta = \pi/2$, it can be seen that $\sigma_{y,*} = -\tau_{xy,*} = -1/Re_D$. The value of the dimensionless momentum function M_*^y is the integral of $\sigma_{y,*}$ along the y_* direction, as indicated in Eq. (29). Different values of the Reynolds number will give different fields of the momentum function M_*^y, but the pattern of the momentum lines of M_*^y remains the same as in Fig. 4b.

3.2. Fully developed laminar flow between parallel plates

The domain under analysis is presented in Fig. 6, and consists of an horizontal channel of width D and length

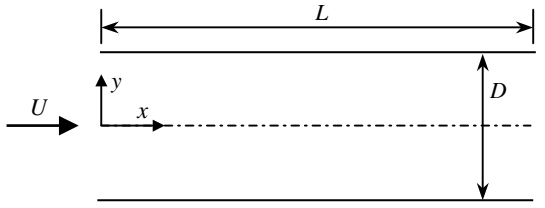

Fig. 6. Physical domain and geometry for the fully developed flow problem between parallel plates.

L, delimited by two parallel plates, where a fluid flows in fully developed laminar regime.

It is well known that, for this problem, $v = 0$ and $(\partial u/\partial x) = 0$ [11]. Under such assumptions the momentum equation in the y direction, Eq. (6), gives $\partial p/\partial y = 0$, and pressure is a function of x only. The momentum equation in the x direction, Eq. (5), becomes $\mathrm{d}p/\mathrm{d}x = \mu(\partial^2 u/\partial y^2)$. As the left side of this relation depends only of x, and the right side depends only of y, each of these terms must be constant, and it can be written that

$$\frac{\mathrm{d}^2 u}{\mathrm{d}y^2} = -\frac{1}{\mu}\left(-\frac{\mathrm{d}p}{\mathrm{d}x}\right) \tag{30}$$

where $-\mathrm{d}p/\mathrm{d}x$ is a constant. This equation can be solved noting that it is $u = 0$ at $y = \pm D/2$, to give the Hagen–Poiseuille solution

$$u = \frac{3}{2}\left[\frac{D^2}{12\mu}\left(-\frac{\mathrm{d}p}{\mathrm{d}x}\right)\right]\left[1 - 4\left(\frac{y}{D}\right)^2\right] \tag{31}$$

y being measured away from the channel centerline. The term within the first square brackets is the average velocity in the channel, usually referred to as $U = [D^2/(12\mu)][-(\mathrm{d}p/\mathrm{d}x)]$. Thus, the average velocity U and the negative of the pressure drop are proportional, and the u velocity profile is parabolic.

For a given mass flow rate, an average velocity U is specified, and so are the Reynolds number, $Re_D = \rho UD/\mu$, and the pressure gradient, which is $-(\mathrm{d}p/\mathrm{d}x) = (12\mu/D^2)U$. Making the velocity dimensionless as $u_* = u/U$, and the co-ordinates dimensionless as $(x_*, y_*) = (x, y)/D$, the dimensionless counterpart of Eq. (35) is

$$u_* = (3/2)\left(1 - 4y_*^2\right) \tag{32}$$

The pressure decreases linearly with x, and its gradient can be expressed as $-(\mathrm{d}p/\mathrm{d}x) = -[p(L) - p(0)]/L$. The reference pressure, p_0, is taken as the minimum pressure value, $p_0 = p(L)$. If pressure is made dimensionless as $p_* = p/(\rho U^2)$, the dimensionless linearly decreasing pressure variation with x_* is

$$(p_* - p_{0,*}) = \left[p_*(0) - p_{0,*}\right] \times [1 - (D/L)x_*] \tag{33}$$

and the dimensionless pressure gradient is

$$-\frac{\mathrm{d}p_*}{\mathrm{d}x_*}=\frac{12}{Re_D} \tag{34}$$

From Eqs. (33) and (34) it is obtained that $[p_*(0)-p_{0,*}]=(12/Re_D)(L/D)$, and Eq. (33) can be rewritten as

$$\left(p_*-p_{0,*}\right)=\frac{12}{Re_D}\left(\frac{L}{D}-x_*\right) \tag{35}$$

In this case the momentum function M^x is defined from Eqs. (8a) and (8b) through $(\partial M^x/\partial y)=\rho uu+(p-p_0)$ and $-(\partial M^x/\partial x)=-\mu(\partial u/\partial y)$ or, if the momentum functions are made dimensionless as $(M^x_*,M^y_*)=(M^x,M^y)/(\rho U^2 D)$, and using Eqs. (32) and (35), as

$$\frac{\partial M^x_*}{\partial y_*}=\frac{9}{4}\left(1-4y_*^2\right)^2+\frac{12}{Re_D}\left(\frac{L}{D}-x_*\right) \tag{36a}$$

$$\frac{\partial M^x_*}{\partial x_*}=-\frac{12}{Re_D}y_* \tag{36b}$$

From Eqs. (36a) and (36b) it is obtained, by integration, the analytical expression for the dimensionless momentum function M^x_* as

$$M^x_*(x_*,y_*)=y_*\left[\frac{9}{4}\left(1-\frac{8}{3}y_*^2+\frac{16}{5}y_*^4\right)+\frac{12}{Re_D}\left(\frac{L}{D}-x_*\right)\right] \tag{37}$$

For this problem, the momentum function M^y is defined from Eqs. (9a) and (9b) through $(\partial M^y/\partial y)=-\mu(\partial u/\partial y)$ and $-(\partial M^y/\partial x)=(p-p_0)$ or, in the dimensionless form, taking present Eqs. (32) and (35),

$$\frac{\partial M^y_*}{\partial y_*}=\frac{12}{Re_D}y_* \tag{38a}$$

$$\frac{\partial M^y_*}{\partial x_*}=-\frac{12}{Re_D}\left(\frac{L}{D}-x_*\right) \tag{38b}$$

From Eqs. (38a) and (38b) it is obtained the analytical expression for the dimensionless momentum function M^y_* as

$$M^y_*(x_*,y_*)=\frac{6}{Re_D}\left[-2x_*\left(\frac{L}{D}-\frac{1}{2}x_*\right)+y_*^2\right] \tag{39}$$

The note following Eq. (29), relative to the eventual use of the simplified y momentum equation to define the y momentum function, also applies in this case.

Results of the momentum functions for this problem, in the form of momentum lines, are presented in Fig. 7a–d. The momentum function M^x_* is symmetric relative to the centerline, for which $y_*=0$, what is an expected result given the symmetry of the flow profile. For $y_*=0$ it is $M^x_*=0$, another expected result nothing that the plane $y_*=0$ is a symmetry plane. The entering momentum in the x direction, through the inertial term ρuu and through the pressure term $(p-p_0)$ is transferred along the channel, and is directed towards the channel walls. For low Reynolds numbers (high viscosity fluids), the momentum transfer to the walls is more intense, and the paths followed by the entering momentum are shorter. As the shear stress is constant at the walls, also the variation of the momentum function is constant there. However, low Reynolds numbers lead to a more intense variation of the momentum function at the walls, as well as to higher overall forces corresponding to the wall–fluid interaction. At the upper wall, the fluid experiences a shear stress in the $-x$ direction (a negative shear stress), and the momentum function decreases along the upper wall. At the lower wall, the shear stress is also in the $-x$ direction (a positive shear stress), and the momentum function increases along it. At the inlet region, the inertia and pressure terms both point in the x direction (corresponding to the left face of the element under analysis), and the momentum function monotonically increases along such a boundary. In this case, as pressure forces are acting in the x direction, the slope of the momentum lines is not zero at the walls.

For this problem, the hydraulic diameter is $D_h=2D$, and the friction factor, constant along the upper and lower walls, is defined as [11]

$$f=\frac{|\tau_{xy}|_{y=\pm D/2}}{(1/2)\rho U^2}=\frac{12}{Re_D}=\frac{24}{Re_{D_h}} \tag{40}$$

It can be seen that the variation of the dimensionless momentum function M^x_* with x_* is directly related with f, noting that, from Eq. (36b),

$$\left|\frac{\partial M^x}{\partial x}\right|_{y=\pm D/2}\times\frac{D}{(1/2)\rho U^2 D}=\frac{12}{Re_D}=\frac{24}{Re_{D_h}}=f \tag{41}$$

In this way, if the momentum function M^x is made dimensionless using the factor $(1/2)\rho U^2 D$ as reference, as in Eq. (40), the variation of the dimensionless momentum function M^x_* with x_* equals the friction factor f. Comparing with what happens in heat transfer, if an overall dimensionless parameter analogue to the overall Nusselt number is defined as the ratio between the forces in the x direction

$$\begin{aligned}X_{0-L}&=\frac{F_x}{F_{\mathrm{ref}}}=\frac{\int_0^L\left(\tau_{xy}\right)_{y=\pm D/2}\mathrm{d}x}{\rho U^2 D}\\&=\left[M^x_*(L/D)-M^x_*(0)\right]_{y_*=\pm 1/2}\end{aligned} \tag{42}$$

that is, this dimensionless overall coefficient equals the overall change of the dimensionless momentum function M^x_* along the considered length L.

The dimensionless momentum function M^y_* is presented in Fig. 7b, through the momentum lines, for $Re_D=1$. Different Reynolds numbers lead to different

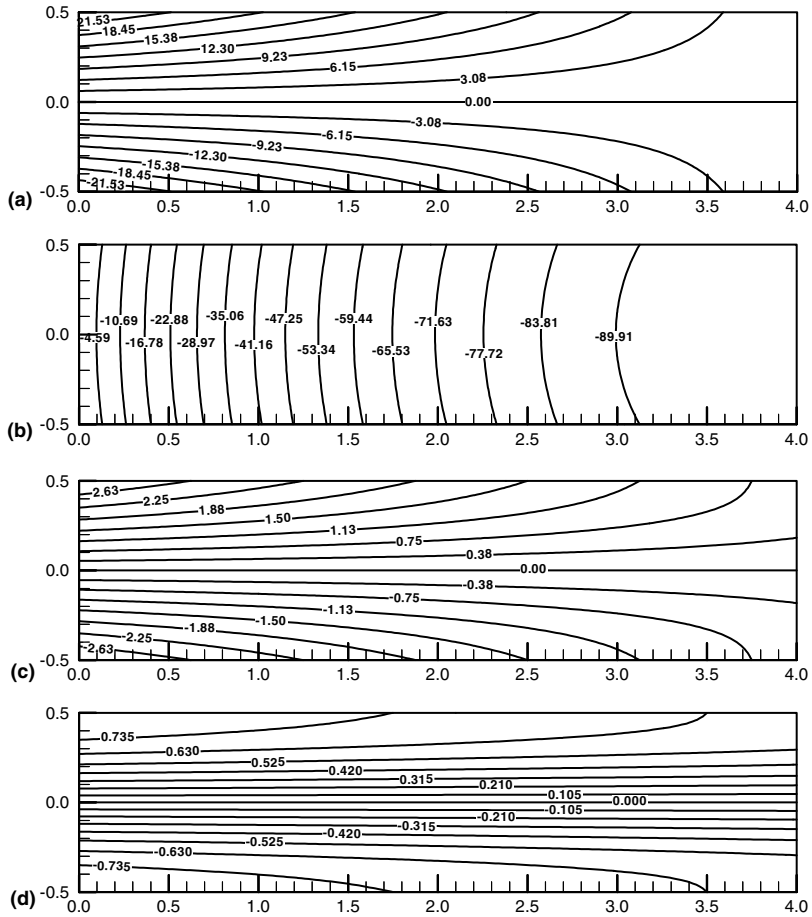

Fig. 7. Dimensionless momentum lines for the fully developed flow problem between parallel plates: (a) momentum lines M_*^x for $Re_D = 1$; (b) momentum lines M_*^y for $Re_D = 1$; (c) momentum lines M_*^x for $Re_D = 10$ and (d) momentum lines M_*^x for $Re_D = 100$.

values of the momentum function, but the pattern of Fig. 7b is maintained. If the vertical shear stress were not present, as is occurs at the centerline of the channel, the momentum lines where vertical. However, as this shear stress is present, and its intensity increases as the walls are closer, the momentum lines are more and more curved as the walls are closer. Along the upper wall, the momentum function decreases, and this decrease occurs through a square profile (Eqs. (38b) and (39)). The momentum function is negative there. This means that, when traveling between two points of the upper wall, there is a force acting over the fluid in the $-y$ direction. This is the resulting force of the action–reaction pair at the upper boundary, where the wall acts over the fluid through a force in the $-y$ direction. This force is due to the pressure, and as the pressure decreases along the channel so decreases this force. This is the reason why the momentum lines become sparser as x_* increases. At the lower wall it occurs a similar situation, noting that at this boundary the wall acts the fluid through a stress that points in the y direction.

3.3. Forced laminar boundary layer flow near a flat plate: similarity solution

When dealing with the laminar boundary layer flow adjacent to a flat plate, as illustrated in Fig. 8, in the usual analysis there are no important pressure changes, and the pressure contribution for the momentum equations can be neglected [11]. Assuming that the boundary layer is thin, $(\delta/L) \ll 1$, the boundary layer momentum equation can be obtained from Eq. (5) as

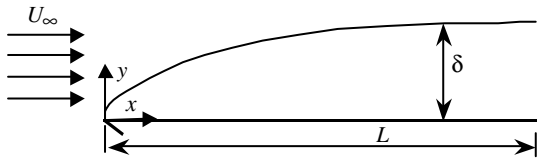

Fig. 8. Physical domain and geometry for the forced laminar boundary layer flow problem.

$$\frac{\partial}{\partial x}(\rho uu)+\frac{\partial}{\partial y}(\rho uv-\tau_{xy})=0 \tag{43}$$

where the shear stress τ_{xx} was neglected when comparing with ρuu, that is, assuming that $\rho uu \gg 2\mu(\partial u/\partial x)$. From scale analysis, this inequality gives $Re_L \gg 2$, where $Re_L=(\rho U_\infty L)/\mu$, a result that is compatible with the boundary layer hypothesis ($Re_L \gg 1$). The shear stress in Eq. (43) is evaluated assuming that, in the boundary layer, $(\partial u/\partial y) \gg (\partial v/\partial x)$. Scale analysis for this inequality gives $\delta/L \ll 1$, also compatible with the boundary layer hypothesis. From scale analysis it is also obtained that $\rho uv \sim \mu(\partial u/\partial y)$, thus resulting in the boundary layer momentum equation [11]

$$\frac{\partial}{\partial x}(\rho uu)+\frac{\partial}{\partial y}\left(\rho uv-\mu\frac{\partial u}{\partial y}\right)=0 \tag{44}$$

It is this momentum equation that will be used to obtain both the flow solution and the momentum function in the boundary layer, by using the similarity transformation, retaining that the boundary layer solution is an approximate solution. In this case, Eq. (44) is the x momentum equation, which includes the simplifications taken for the boundary layer model, and it is thus the momentum equation for the boundary layer taking into account the x and y momentum balances in the boundary layer.

The similarity formulation, for a fluid of constant properties, begins by defining the similarity variable

$$\eta(x,y)=\frac{y}{\delta(x)}=yx^{1/2}Re_L^{1/2}L^{-1/2} \tag{45}$$

where L is the total length of the boundary layer. The streamfunction for this problem is defined as

$$\psi(x,\eta)=\rho U_\infty Re_L^{-1/2}L^{1/2}x^{1/2}f(\eta) \tag{46}$$

where $f(\eta)$ is the dimensionless similarity function to be evaluated. The velocity components are evaluated from the so defined streamfunction as $\rho u=(\partial\psi/\partial y)$ and $\rho v=(-\partial\psi/\partial x)$. Making the space co-ordinates dimensionless as $x_*=x/L$ and $y_*=yRe_L^{1/2}L^{-1}$, and the velocity components dimensionless as $(u_*,v_*)=(u,v)/U_\infty$, it is $\eta(x_*,y_*)=x_*^{-1/2}y_*$, and the dimensionless velocity components can be obtained as

$$u_*=f' \tag{47a}$$

$$v_*=(1/2)Re_L^{-1/2}x_*^{-1/2}(\eta f'-f) \tag{47b}$$

where $f'=\mathrm{d}f/\mathrm{d}\eta$. When these velocity components are introduced into the boundary layer momentum equation, Eq. (44), the following ordinary differential equation is obtained for $f(\eta)$

$$2f'''+ff''=0 \tag{48}$$

subjected to the boundary conditions $f(0)=f'(0)=0$ and $f'(\eta\to+\infty)=1$. The similarity transformation has thus the advantage of reducing the number of independent variables from 2 to 1, and transform a partial differential equation in an ordinary differential equation. Eq. (48) can be solved numerically, and once known the solution for f the flow solution is readily known using Eqs. (47a) and (47b).

The momentum function M^x can be defined, for this simplified case, from Eq. (44) through $(\partial M^x/\partial y)=\rho uu$ and $-(\partial M^x/\partial x)=\rho uv-\mu(\partial u/\partial y)$. Making the momentum function dimensionless as $M_*^x=M^x/(\rho U_\infty^2 LRe_L^{-1/2})$, the dimensionless expressions for the momentum function are

$$\frac{\partial M_*^x}{\partial y_*}=f'^2 \tag{49a}$$

$$-\frac{\partial M_*^x}{\partial x_*}=x_*^{-1/2}\left[\frac{1}{2}(\eta f'^2-ff')-f''\right] \tag{49b}$$

Assuming that the expression for the dimensionless momentum function M_*^x is of the form

$$M_*^x(x_*,\eta)=x_*^n g(\eta) \tag{50}$$

similarly to what was made before for the heatfunction in a laminar forced convection boundary layer [7], the first-order derivatives of M_*^x can be obtained from Eq. (50) and made equal to the expressions given by Eqs. (49a) and (49b), and from the resulting equalities it is extracted that

$$g(\eta)=\frac{1}{n}x_*^{(-n+1/2)}\left(\frac{1}{2}ff'+f''\right) \tag{51}$$

This function is dependent only of η if $n=1/2$, and the expression for the similarity version of the dimensionless momentum function M_*^x becomes

$$M_*^x(x_*,\eta)=x_*^{1/2}(ff'+2f'') \tag{52}$$

with $M_*^x(0,0)=0$. In this way, once known the solution for the similarity function, $f(\eta)$, the solution for the dimensionless momentum function M_*^x is also readily known.

In what concerns the momentum function M^y, it can be defined for this simplified case through $(\partial M^y/\partial y)=\rho uv-\mu(\partial u/\partial y)$ and $-(\partial M^y/\partial x)=\rho vv-2\mu(\partial v/\partial y)$. In this case it is also assumed that $(\partial u/\partial y)\gg(\partial v/\partial x)$ or, in an order of magnitude sense, that $\delta/L\ll 1$ and, as previously mentioned, $\rho uv\sim\mu(\partial u/\partial y)$. Scale analysis also gives that $\rho vv\sim 2\mu(\partial v/\partial y)$. However, a similarity solution for M_*^y, in the form of Eq. (52), cannot be obtained. Thus, the analysis of results will be made taken into account the dimensionless momentum function M_*^x only.

Results of the dimensionless momentum function M_*^x, obtained from Eq. (52), are presented in Fig. 9a (using the dimensionless similarity variable as ordinate) and b (using the dimensionless vertical co-ordinate as

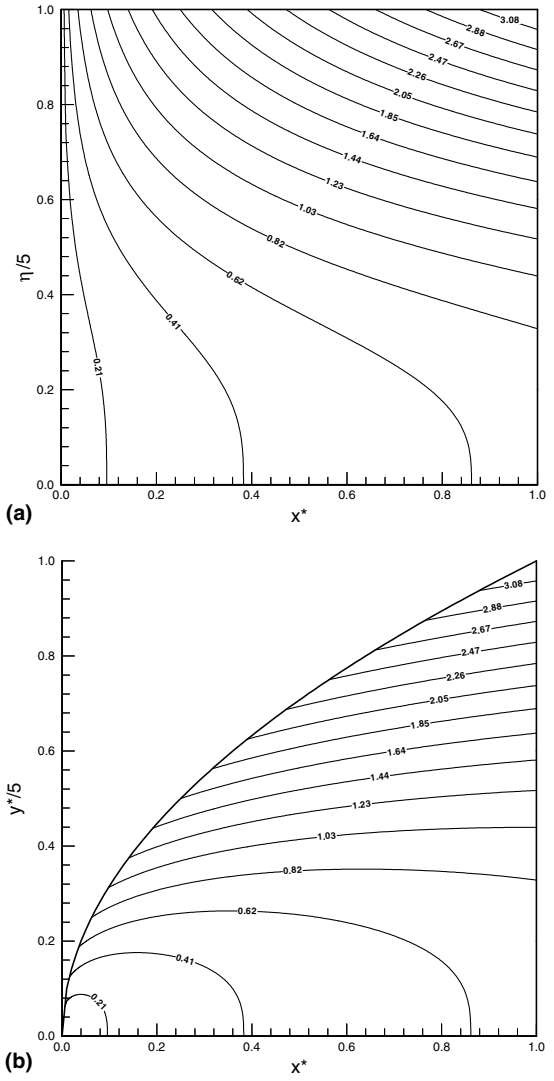

Fig. 9. Dimensionless momentum lines M_*^x for the forced laminar boundary layer flow problem: (a) using $\eta/5$ as ordinate and (b) using $y_*/5$ as ordinate.

ordinate). It should be stressed that these results are formally similar to the ones for the heatfunction obtained for the laminar forced convection boundary layer problem, as presented in [7]. The momentum function increases along the flat plate because, for a bottom surface of an element, a shear force is positive when it points in the $-x_*$ direction. It can be seen also that the shear force is more intense near the leading edge of the flat plate, the momentum lines being sparser for positions of the flat plate with higher values of x_*. In particular, Fig. 9b is very rich, showing as the momentum of the free stream is entrained by the boundary layer, and how this momentum reaches the flat plate, in the form of a shear stress pointing in the $-x_*$ direction. In this case, as it is $(\partial M_*^x/\partial y_*)_{y_*=0} = 0$, the slope of the momentum function is null at the flat plate, for $y_* = 0$.

The local skin-friction coefficient is obtained as [11]

$$C_{f,x} = \frac{\left[\mu(\partial u/\partial y)_{y=0}\right]_x}{(1/2)\rho U_\infty^2} = 2(f'')_{\eta=0} Re_x^{-1/2} \tag{53}$$

where $Re_x = \rho U_\infty x/\mu$, and from Eq. (49b) it can be obtained that

$$\frac{\partial M^x}{\partial x} \times \frac{L}{(1/2)\rho U_\infty^2 L} = 2(f'')_{\eta=0} Re_x^{-1/2} = C_{f,x} \tag{54}$$

where $(f'')_{\eta=0} = 0.332$. In this way, if the momentum function is made dimensionless in the adequate way, its variation with x_* equals the local skin-friction coefficient. Also in this case it can be used an overall dimensionless parameter to quantify the overall force acting in the x direction in the fluid-wall interface, similarly to what was referred in Section 3.2.

3.4. Laminar forced flow in a channel with an obstacle

In this case the domain under analysis is the half channel presented in Fig. 10. The half channel has width D and length L, and includes an obstacle of length L_{ob} and height H_{ob}, which is placed at a distance x_{ob} measured away from the inlet. The lower boundary of the half channel is a symmetry plane. In particular, it was considered a channel with the following geometrical parameters: $L/D = 4$, $H_{ob}/D = 0.25$, $L_{ob}/D = 0.20$, and $x_{ob}/D = 1$.

The flow problem is taken in the dimensionless form through the dimensionless mass conservation and momentum differential equations

$$\frac{\partial u_*}{\partial x_*} + \frac{\partial v_*}{\partial y_*} = 0 \tag{55}$$

$$\frac{\partial}{\partial x_*}(u_* u_*) + \frac{\partial}{\partial y_*}(v_* u_*) = -\frac{\partial (p - p_0)_*}{\partial x_*} + \frac{1}{Re_D}\left(\frac{\partial^2 u}{\partial x_*^2} + \frac{\partial^2 u}{\partial y_*^2}\right) \tag{56a}$$

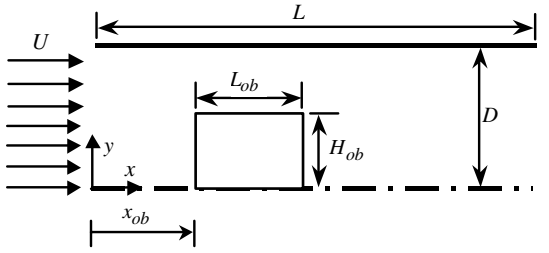

Fig. 10. Physical domain and geometry for the flow problem in a channel with an obstacle.

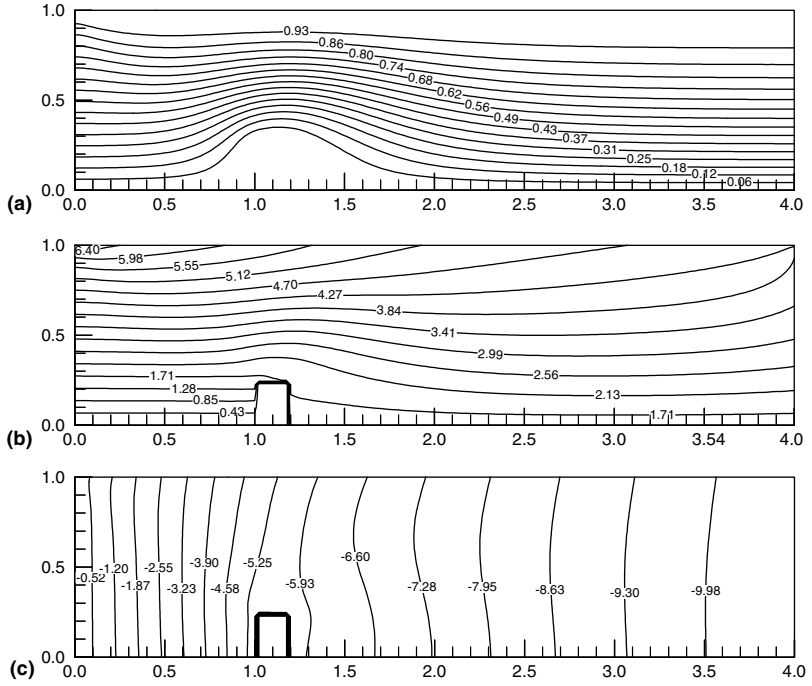

Fig. 11. Dimensionless results for the flow problem in a channel with an obstacle, for $Re_D = 10$: (a) stream lines; (b) momentum lines M_*^x; and (c) momentum lines M_*^y.

$$\frac{\partial}{\partial x_*}(u_* v_*) + \frac{\partial}{\partial y_*}(v_* v_*) = -\frac{\partial (p - p_0)_*}{\partial y_*} + \frac{1}{Re_D}\left(\frac{\partial^2 v}{\partial x_*^2} + \frac{\partial^2 v}{\partial y_*^2}\right) \tag{56b}$$

where the co-ordinates are made dimensionless as $(x_*, y_*) = (x, y)/D$, the velocity components as $(u_*, v_*) = (u, v)/U$, the pressure as $p_* = p/(\rho U^2)$, and the Reynolds number $Re_D = \rho UD/\mu$ is based on the width D.

Once known the flow solution, obtained using a 2D laminar version of the control volume finite element method presented in [19], the momentum functions can be evaluated as the solution of Eqs. (15) and (17). Making the momentum functions dimensionless as $(M_*^x, M_*^y) = (M^x, M^y)/(\rho U^2 D)$, the dimensionless version of Eqs. (15) and (17) become

$$\frac{\partial^2 M_*^x}{\partial x_*^2} + \frac{\partial^2 M_*^x}{\partial y_*^2} = -\frac{\partial (u_* v_*)}{\partial x_*} + \frac{\partial (u_* u_*)}{\partial y_*} + \frac{\partial (p - p_0)_*}{\partial y_*} - \frac{1}{Re_D}\frac{\partial}{\partial x_*}\left(\frac{\partial u_*}{\partial y_*} - \frac{\partial v_*}{\partial x_*}\right) \tag{57a}$$

$$\frac{\partial^2 M_*^y}{\partial x_*^2} + \frac{\partial^2 M_*^y}{\partial y_*^2} = -\frac{\partial (v_* v_*)}{\partial x_*} + \frac{\partial (u_* v_*)}{\partial y_*} - \frac{\partial (p - p_0)_*}{\partial x_*} - \frac{1}{Re_D}\frac{\partial}{\partial y_*}\left(\frac{\partial u_*}{\partial y_*} - \frac{\partial v_*}{\partial x_*}\right) \tag{57b}$$

Some of the results obtained for this problem are presented in Fig. 11a–c for $Re_D = 10$ and in Fig. 12a–c for $Re_D = 100$. Fig. 11a presents the stream lines, and thus the topology of the flow. In Fig. 11b are presented the dimensionless momentum lines of M_*^x. It is observed the momentum inlet, essentially through the inertia and pressure terms. Some of this entering momentum is lost *against* the obstacle. At the lower boundary there are no forces in the x direction, as the plane $y_* = 0$ is a symmetry plane. At the upper surface it is observed how part of the entering momentum is transferred to this wall. The momentum function values decrease along the upper boundary, thus meaning that the upper surface acts over the fluid through shear stresses pointing in the $-x$ direction. In what concerns the dimensionless momentum function M_*^y, presented in Fig. 11c, it presents a profile with some similitude with this presented in Fig. 7b, and the reasons are essentially the same as explained when analyzing Fig. 7b.

Results for $Re_D = 100$ are presented in Fig. 12a–c. Stream lines, in Fig. 12a, show a larger region of the flow behind the obstacle being affected by it. The main pattern of the momentum function M_*^x remains as for the case of $Re_D = 10$ (Fig. 11b). It should be noted, however, that a higher value of the Reynolds number can be interpreted as a fluid of lower viscosity, and the involved forces in the x direction are lower than for $Re_D = 10$, as given by the dimensionless values of the momentum function M_*^x. At

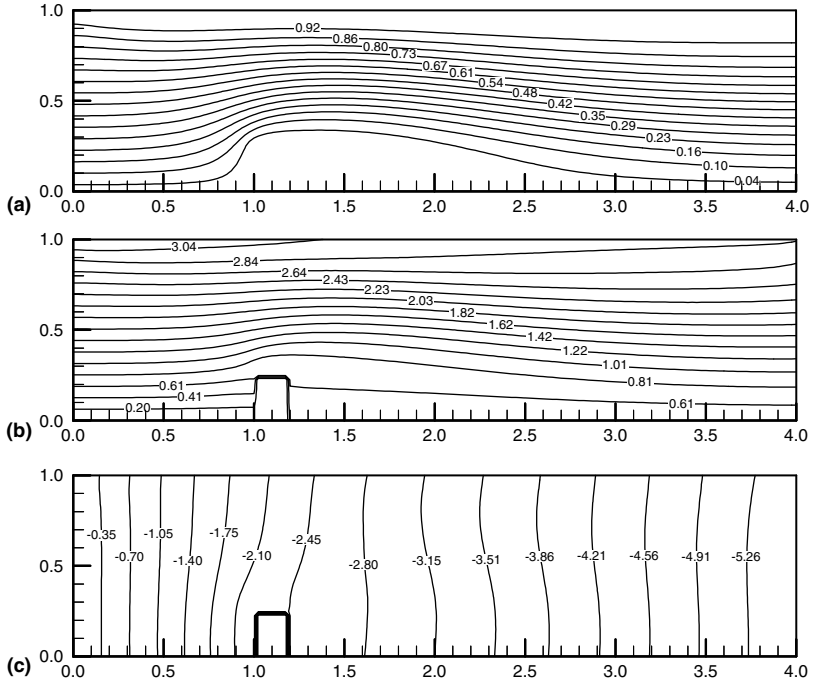

Fig. 12. Dimensionless results for $Re_D = 100$. Base legend as for Fig. 11.

the upper boundary the momentum lines for M_*^x are thus sparser for $Re_D = 100$ than for $Re_D = 10$.

In what concerns the dimensionless momentum function M_*^y, presented through the dimensionless momentum lines in Fig. 12c, its pattern is essentially the same as in Fig. 11c. However, for a fluid with higher Reynolds number the involved forces in the x direction are lower, and it is also lower the pressure decrease along the channel, as given by the momentum lines in Fig. 12c.

4. Conclusions

Convective heat and/or mass transfer processes can be visualized and analyzed using the heatfunction and the heat lines and/or using the massfunction and mass lines. Similarly, the momentum functions can be defined for two-dimensional steady flows, and their contour plots, the momentum lines, can be used for flow visualization and analysis. Streamfunction and stream lines give a good picture about the topology of the flow, but not relevant information about the forces present within the fluid and at the interfaces between the fluid and the walls containing it. Momentum functions and momentum lines give very useful information about these interactions, in the form of forces.

Due to the vector nature of forces, two momentum functions need to be defined, associated with the x and y Cartesian co-ordinate directions. Over the momentum lines there are no stresses or forces in one co-ordinate direction, and the region between two momentum lines can be seen as a beam in which surface there are no stresses or forces in that co-ordinate direction under analysis. It is well known that care needs to be taken when analyzing the state of stress at a point, as the involved forces are dependent of the orientation of the surface under analysis. This same care should be present when dealing with the momentum functions and momentum lines, as they are closely related with the state of stress at a point.

Momentum functions can be used to obtain momentum arrows' pictures. For the worked examples, however, the message given by the momentum lines is much more clear about the involved forces than that given by the momentum arrows.

Presented results, for relatively simple flow problems, show new pictures towards a better understanding, visualization and quantification of the forces involved with fluid flow. With these pictures, closer comparisons can be made between the heat and/or mass transfer processes and the momentum transfer processes. When made dimensionless in the adequate way, the momentum functions are closely related with the skin-friction coefficient that characterizes the overall wall–fluid interaction in terms of forces, which is one of the most relevant parameters for engineering purposes.

When dealing with markedly recirculating flows, pictures given by the momentum lines are not usually so

clear, as the pressure term increases in importance. In this case, the main information obtained from the momentum lines is that opposed walls support pressure forces, and only small effects arise in the momentum lines associated with the (usually more important from the engineering viewpoint) shear stresses at the walls. However, further work will result in improvements of the method.

Acknowledgments

The author wish to thank one anonymous reviewer, who suggested the use of the momentum arrows for momentum visualization and analysis.

References

[1] S. Kimura, A. Bejan, The "heat line" visualization of convective heat transfer, ASME J. Heat Transfer 105 (1983) 916–919.
[2] E.R.G. Eckert, R.M. Drake Jr., Analysis of Heat and Mass Transfer, McGraw-Hill, New York, 1972.
[3] O.V. Trevisan, A. Bejan, Combined heat and mass transfer by natural convection in a vertical enclosure, ASME J. Heat Transfer 109 (1987) 104–112.
[4] D. Littlefield, P. Desai, Buoyant laminar convection in a vertical cylindrical annulus, ASME J. Heat Transfer 108 (1986) 814–821.
[5] S.K. Aggarwal, A. Manhapra, Use of heat lines for unsteady buoyancy-driven flow in a cylindrical enclosure, ASME J. Heat Transfer 111 (1989) 576–578.
[6] S.K. Aggarwal, A. Manhapra, Transient natural convection in a cylindrical enclosure nonuniformly heated at the top wall, Numer. Heat Transfer, Part A 15 (1989) 341–356.
[7] Al.M. Morega, A. Bejan, Heat line visualization of forced convection boundary layers, Int. J. Heat Mass Transfer 36 (1993) 3957–3966.
[8] Al.M. Morega, A. Bejan, Heat line visualization of forced convection in porous media, Int. J. Heat Fluid Flow 15 (1994) 42–47.
[9] V.A.F. Costa, Heat line and mass line visualization of the laminar natural convection boundary layers near a vertical wall, Int. J. Heat Mass Transfer 43 (20) (2000) 3765–3774.
[10] S.K. Dash, Heat line visualization in turbulent flow, Int. J. Numer. Meth. Heat Fluid Flow 5 (1996) 37–46.
[11] A. Bejan, Convection Heat Transfer, second ed., Wiley, New York, 1995.
[12] V.A.F. Costa, Unification of the stream line, heat line and mass line methods for the visualization of two-dimensional transport phenomena, Int. J. Heat Mass Transfer 42 (1) (1999) 27–33.
[13] V.A.F. Costa, Unified stream line, heat line and mass line methods for the visualization of two-dimensional heat and mass transfer in anisotropic media, Int. J. Heat Mass Transfer 46 (8) (2003) 1309–1320.
[14] A. Mukhopadhyay, X. Qin, S.K. Aggarwal, I.K. Puri, On extension of "heat line" and "mass line" concepts to reacting flows through use of conserved scalars, ASME J. Heat Transfer 124 (2002) 791–799.
[15] A. Mukhopadhyay, X. Qin, I.K. Puri, S.K. Aggarwal, Visualization of scalar transport in nonreacting and reacting jets through a unified "heat line" and "mass line" formulation, Numer. Heat Transfer, Part A 44 (2003) 683–704.
[16] V.A.F. Costa, Bejan's heat lines and mass lines for convection visualization and analysis, Appl. Mech. Rev., in press.
[17] R.B. Bird, W.E. Stewart, E.N. Lightfoot, Transport Phenomena, Wiley, New York, 1960.
[18] V.S. Arpaci, P.S. Larsen, Convection Heat Transfer, Prentice-Hall, Englewood Cliffs, NJ, 1984.
[19] V.A.F. Costa, L.A. Oliveira, A.R. Figueiredo, A control volume based finite element method for three-dimensional incompressible turbulent fluid flow, heat transfer, and related phenomena, Int. J. Numer. Meth. Fluids 21 (7) (1995) 591–613.